BITalino
A Multimodal Platform for Physiological Computing

José Guerreiro[1,2], Raúl Martins[1], Hugo Silva[1], André Lourenço[1,2] and Ana Fred[1]
[1]*Instituto de Telecomunicações, Instituto Superior Técnico, Avenida Rovisco Pais, 1, 1049-001 Lisboa, Portugal*
[2]*Instituto Superior de Engenharia de Lisboa, Rua Conselheiro Emídio Navarro, 1, 1959-007 Lisboa, Portugal*

Keywords: Biomedical Instrumentation, Biosignal Acquisition, Electrocardiography, Electromiography, Electrodermal Activity, Accelerometry, Light Sensing.

Abstract: By definition, physical computing deals with the study and development of interactive systems that sense and react to the analog world. In an analogous way, physiological computing can be defined as the field, within physical computing, that deals with the study and development of systems that sense and react to the human body. While physical computing has seen significant advancements leveraged by the popular Arduino platform, no such equivalent can yet be found for physiological computing. In this paper we present a novel, low-cost and versatile platform, targeted at multimodal biosignal acquisition and that can be used to support classroom activities, interface with other devices, or perform rapid prototyping of end-user applications in the field of physiological computing. We build on previous work developed by our group, by presenting an improved version of the BITalino platform, emphasizing on the hardware characterization, benchmarking and design principles.

1 INTRODUCTION

Today, biosignals are increasingly gaining attention beyond the classical medical domain, into a paradigm, which using the physical computing analogy (O'Sullivan and Igoe, 2004), can be described as physiological computing. The modern uses of biosignals have become an increasingly important topic of study within the global engineering community and consequently, many evidences show that biosignals are clearly a growing field of interest; recent applications include: Human-Computer Interaction (HCI), which involve the interface between the user and the computer (Graimann et al., 2011); Quantified-self, giving people new ways to deal with medical problems or improve their quality of life; and many other disciplines.

Our first approach to the BITalino targeted the integration of an Arduino, together with a series of other off-the-shelve components, and a single Electrocardiographic (ECG) sensor into a system, that allowed real-time acquisition (Alves et al., 2013). In this paper we extend this preliminary work, by presenting a more generic acquisition platform that enables the acquisition of multiple physiological signals, namely Electrocardiography (ECG), Electromiography (EMG), Electrodermal Activity (EDA), and Accelerometry (ACC). Additionaly, it also provides a Light sensor and a Light-Emitting Diode (LED).

We developed analog signal conditioning circuitry adapted for each of the acquired signals (in terms of gain and bandwidth). The analog signals are then fed to a digital back-end consisting of a Micro-controller Unit (MCU - AVR 8-bit RISC), which is directly connected to a Class II Bluetooth v2.0 module (EGBT-045MS). The BITalino platform also includes a low-drop voltage regulator (3.3V) powered by a single Lithium Ion Polymer battery with nominal voltage of 3.7V and 400mAh. For system status and battery information a white and red LED, respectively, were also included, and finally, the clock speed of the system is sourced by an 8MHz external crystal with $\pm 20 ppm$ of frequency stability.

By default, the platform comes as a single board (Figure 1), with its onboard sensors pre-connected to analog and digital ports on the control block. However, it is designed in such way that each individual block can be physically detached from the main board, allowing people to use it in many different configurations. We developed a custom firmware, designed to command the behaviour of the BITalino,

Guerreiro J., Martins R., Silva H., Lourenço A. and Fred A..
BITalino - A Multimodal Platform for Physiological Computing.
DOI: 10.5220/0004594105000506
In *Proceedings of the 10th International Conference on Informatics in Control, Automation and Robotics* (ICINCO-2013), pages 500-506
ISBN: 978-989-8565-70-9

and configure multiple acquisition parameters.

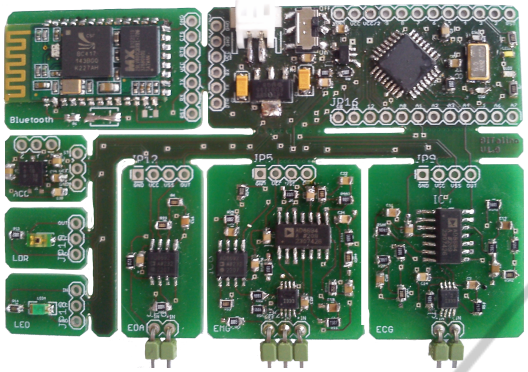

Figure 1: The BITalino platform.

The remainder of the paper is organized as follows: Section 2 describes the analog front-end; Section 3 describes the data handling firmware logic; Experimental results are summarized in Section 4, and finally, we outline the main conclusions and future work in Section 5.

2 ANALOG FRONT-END

In this section we describe each of the sensors (ECG, EMG, EDA, ACC, LDR) and the actuator (LED) that the BITalino platform integrates. Each sensor is single-ended and was designed according to the nature of the signal. There are different types of measurement principles that can be used, namely: electrical potentials, such as ECG and EMG signals (Malmivuo, 1995), (Webster, 2009); resistance, such as EDA signals (Boucsein, 2011); and biomechanics (Winter, 2004). Table 1 summarizes a few of the commonly used physiological signals which were the basis for our design (Webster, 2009), (Merlo and Campanini, 2010), (Myong-Woo Lee, 2011).

Table 1: A few commonly used physiological signals.

Modality	Range	Frequency
ECG	$0.5-4mV$	$0.01-250Hz$
EMG	$0.1-5mV$	$10-400Hz$
EDA	$1-500k\Omega$	$0.01-1Hz$
ACC	$\pm 1.5G$	$0-10Hz$

2.1 ECG and EMG

The ECG and EMG sensors are based on voltage potential differential principles. Accordingly, to measure the low potential differences associated with these signals (in the mV range), both include a precision instrumentation amplifier (In-Amp), offering high common-mode rejection (110dB at G $\geq$ 10). Also, they have low-noise high speed operational amplifiers (Op-Amp) to perform bandpass filtering and amplification.

On one hand, the ECG sensor was designed for 1-lead measurement of the bioelectrical activity of the heart, and it is specially designed for fingers or hands electrode placement. However, it is also possible use the sensor in the standard locations (e.g. chest). A block diagram of the ECG sensor circuit can be seen in Figure 2, and its frequency response is shown in Figure 3. Equation 1 shows the transfer function for this sensor.

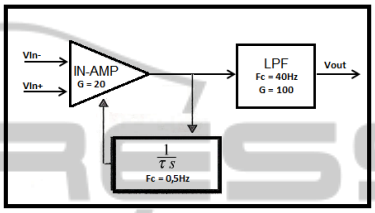

Figure 2: Block diagram of the ECG sensor block; an In-Amp with AC coupling to reject DC input voltages, followed by a Butterworth 4^{th} order lowpass filter.

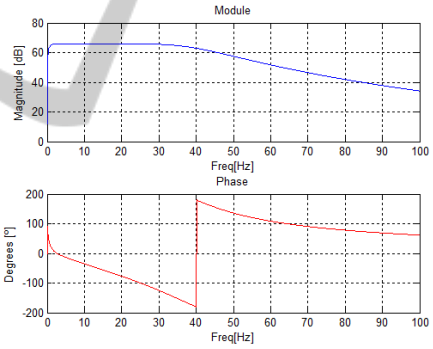

Figure 3: Frequency response of the ECG sensor.

$$V_{out} = (V_{IN+} - V_{IN-}) \times 2000 + V_{ss} \quad (1)$$

On the other hand, the EMG sensor is used for measuring the bioelectrical activity from the muscles, and may be applied to any surface muscle found in the standard locations (Hermens et al., 2000), (Basmajian and De Luca, 1985). A block diagram of the EMG sensor circuit can be seen in Figure 4, and its frequency response is shown in Figure 5. Equation 2 shows the transfer function for this sensor.

$$V_{out} = (V_{IN+} - V_{IN-}) \times 1000 + V_{ss} \quad (2)$$

2.2 EDA

The EDA sensor was designed for measuring skin resistance, namely, the galvanic skin level and the galvanic skin response. In which case the electrodes

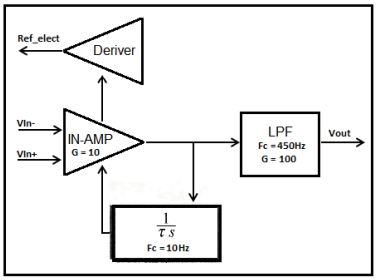

Figure 4: Block diagram of the EMG sensor block; an In-Amp with AC coupling to reject DC input voltages, followed by a Butterworth 4^{th} order lowpass filter; a circuit to deriving common-mode voltage is used to invert the common-mode signal and drive it back into the user through the reference electrode.

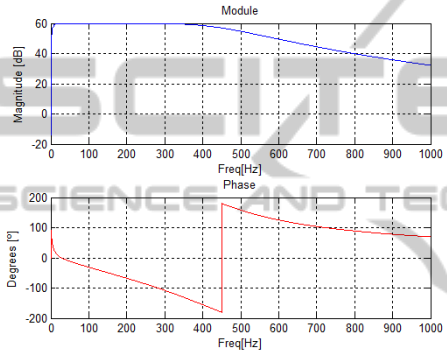

Figure 5: Frequency response of the EMG sensor block.

are applied at the hand palms or fingers, allowing the measurement of the variations in the skin resistance originated by sweat duct secretion activity. This sensor is based on an Operational Transcondutance Amplifier (OTA) circuit, whose input voltage produces an output current. The block diagram of this circuit is shown in Figure 6.

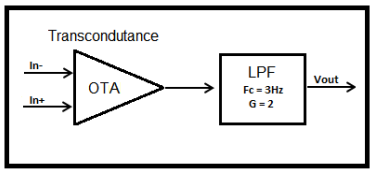

Figure 6: Block diagram of the EDA sensor block; an OTA followed by a 1^{st} order lowpass filter.

Equation 3 shows the transfer function of this circuit.

$$V_{out} = (-\frac{R_{skin}}{R} \times V_{cc} + \frac{R+R_{skin}}{R} \times V_{ss}) \times G \quad (3)$$

As described in (Boucsein, 2011), the typical skin resistance values range between $1k\Omega \leq R_{skin} \leq 500k\Omega$ when injecting a DC current. Assuming $R = 500k\Omega$ then:

- $R_{skin} = 1k\Omega \longrightarrow V_{out} \simeq V_{cc}$;
- $R_{skin} = 500k\Omega \longrightarrow V_{out} \simeq 0$.

The value of the resistance R defines the value of the current injected in the user skin. In this case we assume that $V_{cc} = 3.3V$, then:

$$I_{skin} = \frac{3.3V}{500k\Omega} = 6.6\mu A \quad (4)$$

Considering a sampling resolution of 10 bits, then:

$$\triangle V = \frac{3.3V}{2^{10}} = 3.2mV \quad (5)$$

As such, the resistance resolution of the circuit is:

$$\triangle C = \frac{I_{skin}}{\triangle V} = \frac{6.6\mu A}{3.2mV} = 2.06m\Omega^{-1} \longrightarrow \triangle R = 485\Omega \quad (6)$$

As highlighted in Equation 6, the resolution of the circuit is delimited by the value of the injected current.

2.3 Other Features

In order to maximize the range of applications and provide a more versatile platform. BITalino also integrates an accelerometer, a light sensor and a LED. The accelerometer can be used for measuring biomechanical events (e.g. walking patterns, step counting, or physical activity). To enable the creation of a complete 3-axis acceleration measurement system, a small and low power accelerometer module was used (ADXL335), allowing a full-scale range of $\pm 3G$ and analog outputs. In our design, the bandwidth was selected with a range of $0.5 - 50Hz$ for all axis (x, y, z).

The light sensor can be used for optical synchronization with external sources or for ambient light sensing. This sensor acts as an NPN transistor (photo transistor); the more the sensor is exposed to light, the stronger is the base bias. The device is sensitive to the spectral bandwidth range of $360 - 970nm$. Finally, the LED actuator can be used for synchronization with image capture external devices.

3 FIRMWARE

As previously mentioned, the firmware defines the overall behaviour of the system, and controls the data streaming over Bluetooth. The system allows the acquisition of 6 analog input ports (4 with 10 bit + 2 with 6 bit), and also exposes 8 digital ports (4 input + 4 output). The system has three operation modes, and has a set of commands that can be used to configure the device. The global operation workflow is represented in Figure 7.

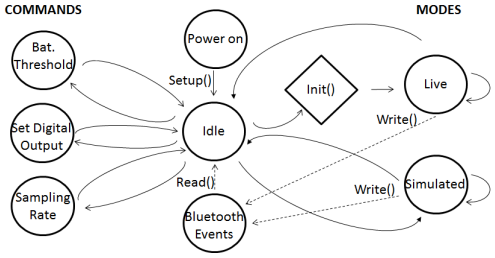

Figure 7: State diagram of the firmware operation.

The configurable settings on the system are changed by sending 1 byte commands from the base station to the device; Figure 8 summarizes the modes and commands that are recognized by the system.

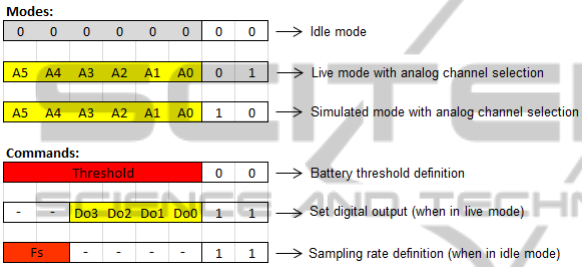

Figure 8: Modes and commands of the system operation.

3.1 Modes

a) *Idle*: The system disables any mode in which it is in, and stays in standby until it receives a command from the base station to change mode or adjust settings;

b) *Live*: In this mode, the system continuously samples all input analog and digital channels, packs the data into a set of bytes, and sends the data packets through the USART controller. In order to make the most efficient use of the available bandwidth on the communication channel, the packet is optimized and its size depends on the number of channels acquired in each period. The packet has a maximum size of 8 bytes and a minimum size of 3 bytes; it includes also a sequence number and a 4-bit Cyclic Redundancy Check (CRC), based on a Linear Feedback Shift Register (LSFR) function, to enable the detection of possible errors in the message. This packing process is done using bitwise operators, and the packet structure can be seen in Figure 9.

c) *Simulated*: Although it is similar to what is done in the *Live* mode; in this mode the system will simulate the acquisition, transmitting synthesized signals. These correspond to sinusoidal (A2-A4) and square waves (D0-D3), white noise (with Normal Distribution) (A1) and a synthetic ECG wave (A0). The data packet structure is the same as before. This way, the communication and interaction between the base station and the device can be tested, without having the system connected to a user.

Bytes	Bits 7	6	5	4	3	2	1	0
0	S	S	S	S	CRC	CRC	CRC	CRC
1	D0	D1	D2	D3	A0	A0	A0	A0
2	A0	A0	A0	A0	A0	A0	A1	A1
3	A1	A1	A1	A1	A1	A1	A1	A1
4	A2	A2	A2	A2	A2	A2	A2	A2
5	A2	A2	A3	A3	A3	A3	A3	A3
6	A3	A3	A3	A3	A4	A4	A4	A4
7	A4	A4	A5	A5	A5	A5	A5	A5

Figure 9: Data packet structure.

3.2 Commands

a) *Threshold*: This command is used to define the threshold for the low battery LED indication. One of the analog input ports (A5) is continuously acquiring the voltage level of the battery; when the level is lower than the threshold initially defined, the red LED integrated in the system is turned on.

b) *Set Digital Output*: With this command, the system activates or deactivates the physical digital output ports, according to the information on the channel mask.

c) *Sampling Rate*: This command is used to define the sampling rate for data acquisition; Table 2 presents the valid options for this command.

Table 2: Sampling rate definitions.

Sampling Rate	$1000Hz$	$100Hz$	$10Hz$	$1Hz$
$\mathbf{10}^{Fs}$	10^3	10^2	10^1	10^0

3.3 Real-time Acquisition

The most important requirement on the *Live* mode is the sampling rate accuracy. The approach followed in our work was based on timer interrupts, and as such two Interrupt Service Routines (ISRs) were implemented on Timer 1 and 2, respectively, as illustrated in Figure 10.

The ISR on Timer 1 (16 bits) defines the sampling rate, and it is programmed to set the ADC, sample each channel, and fill a circular buffer (FIFO). On the other hand, the ISR on Timer 2 (8 bits) gets the samples from the buffer, packs all the data and calculates the CRC before sending the data packets through the USART controller, and consequently to Bluetooth module.

Both are programmed in Clear Timer on Compare (CTC) match mode. It is extremely important that the samples inside the buffer are retrieved quicker than they are placed; as such, Timer 2 requires a system call to occur 4 times more frequently than Timer 1 does. Otherwise, there would be an overflow inside the buffer, and consequently the data would be corrupted.

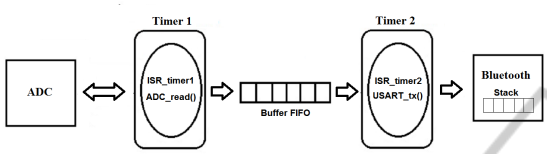

Figure 10: State diagram of the acquisition process.

4 EXPERIMENTAL EVALUATION

Tests were performed to the final system, to check both the digital and analog components, namely, the dynamic specifications of the Analog-to-Digital Conversion (ADC), and the quality of the analog front-end (SNR: Signal-to-Noise Ratio, ENOB: Effective Number of Bits, SINAD: Signal-to-Noise Ratio plus Distortion and THD: Total Harmonic Distortion). In all experimental tests, the signals were generated using an Agilent 33220A function generator.

4.1 Analog-to-Digital Conversion

To characterize the temporal uncertainty of the system, a synthesized ramp wave with a frequency of $10kHz$, with $3V_{pp}$ and offset of $V_{cc}/2$ was acquired, and the data was analysed. The dynamic specifications of the ADC function was also characterize and a synthesized sine wave with a frequency of $15Hz$, with 95% of $3.3V_{pp}$ and offset of $V_{cc}/2$ was used for this purpose. In Table 3 we summarize the sampling rate accuracy results; only the high sampling rates were tested as they are the most demanding in terms of sampling accuracy.

Table 3: Temporal uncertainty of the system.

Fs (ideal value)[Hz]	Fs (real value)[Hz]	skew [%]	jitter [%]
1000	999.9989 ± 0.138	0.00011	0.0138
100	99.9988 ± 0.03	0.00121	0.03

In Table 4 we show the results of the ADC dynamic specifications when the sampling rate is $1000Hz$ and $100Hz$.

The crosstalk between channels was also measured, and it is less than $-105.95dB$.

Table 4: Dynamic specifications of the ADC ($15Hz$ sine wave; Fs = $1kHz$).

SNR [dB]	SINAD [dBc]	THD [dBc]	ENOB [bits]
55.72	54.29	-59.80	8.73

4.2 ECG and EMG

To characterize the real response of the analog circuits (ECG and EMG), we reduced the gain to 100 (INAMP with Gain = 1), to ensure a desirable output signal between $0-3.3V$. In Figures 11 and 12 we show the frequency response of the ECG and EMG circuits. As illustrated in the plots (on top) of these figures, the output signal is a chirp wave with $\approx 2.8V_{pp}$ and with attenuation in low and high frequencies, which is typical in the filter we applied (bandpass filter). During this evaluate test, a synthesized chirp wave with frequencies between $0-100Hz$ and $0-500Hz$, respectively, duration of 1 second, and $28mV_{pp}$ and offset of $V_{cc}/2$ was applied.

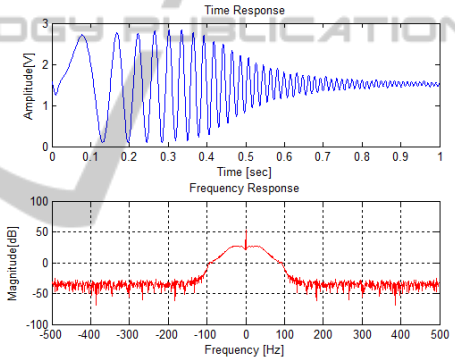

Figure 11: Frequency response of the ECG sensor.

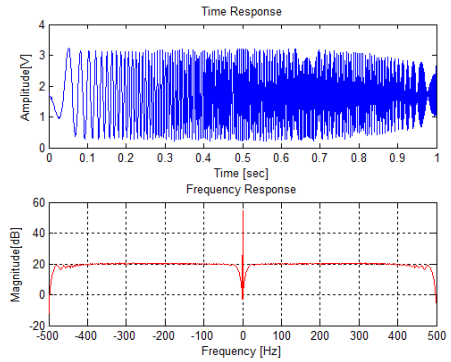

Figure 12: Frequency response of the EMG sensor.

To characterize the dynamic specifications of the analog circuits (ECG and EMG), a synthesized sine wave with a frequency of $24Hz$ and $55Hz$, respectively, with $28mV_{pp}$ and offset of $V_{cc}/2$ was used. Table 5 summarizes the results of the dynamic specifications of the circuits.

Table 5: Dynamic specifications (ECG and EMG, Fs = $1kHz$).

Sensor	SNR [dB]	SINAD [dBc]	THD [dBc]
ECG	44.54	42.49	-46.74
EMG	34.85	34.75	-51.24

In order to measure the time delay of the circuits, a transient analysis was performed and thus, 2.337 seconds is the time delay of the ECG design and 0.146 seconds is the time delay of the EMG design. Finally, real ECG and EMG signals were acquired. For the ECG, we placed the electrodes between the left and right arms and using dry electrodes, and for EMG measurement we placed the sensor over a muscle (biceps brachii) using pre-gelled electrodes, Figures 13 and 14 show examples of real-world data collected with our sensors.

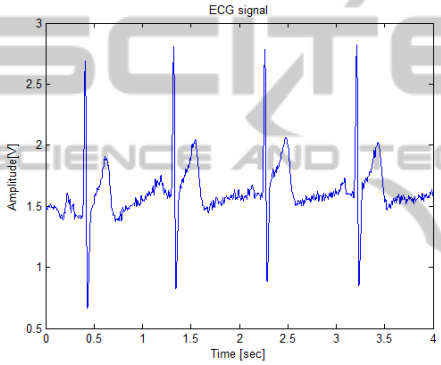

Figure 13: Example of an ECG signal.

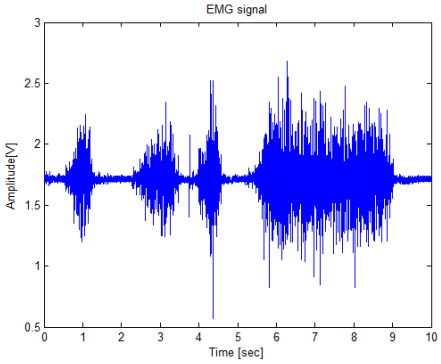

Figure 14: Example of an EMG signal.

4.3 EDA and ACC

The full-scale range of the EDA circuit was tested experimentally, and shown to be able to measure resistances between $0\Omega \leq R_{skin} \leq 500k\Omega$, as expected. Figure 15 shows an example of the signal acquired using this sensor. The ACC sensor was also tested, and in Figure 16 we present a sample of a signal acquired from the z axis during a walking task, in which the BITalino board was carried in the pocket(right leg).

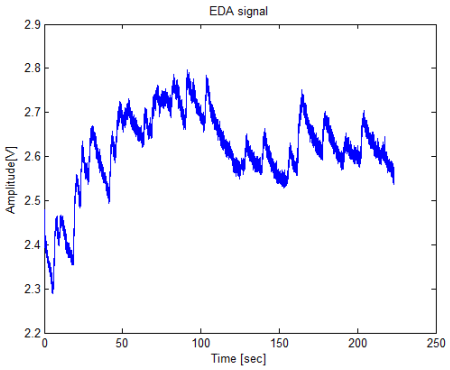

Figure 15: Example of an EDA signal.

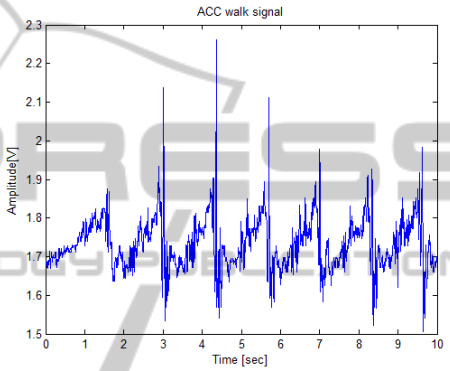

Figure 16: Example of an accelerometry signal.

5 CONCLUSIONS

Our work presents a versatile and low-cost (below €100) platform, which consists of a hardware device with a "Credit Card" form factor, that integrates multiple measurement sensors for biosignal data acquisition, namely, Electrocardiography (ECG), Electromiography (EMG), Electrodermal Activity (EDA), Accelerometry (ACC). It also includes a Light sensor and a Light-Emitting Diode (LED). We believe that BITalino is an important contribution for the research community, as it integrates various types of biosignal sensors in a single board in a way that no other platform does.

The experimental results have shown that the data collected through the proposed system preserves the waveform properties, that the system is accurate for real-time data acquisition, and that the analog front-end behaves according to what is defined in the reference literature as the characteristics of each signal.

Future work will be focused on revising the analog front-end for some of the sensors, improving the form factor of the device into a more flexible platform, integrating an on-board charge management controller to ensure a Lithium-Ion/Lithium-Polymer battery charg-

ing, and on experimenting with Bluetooth Low Energy (BLE), to ensure lower power consumption.

ACKNOWLEDGEMENTS

This work was partially funded by the Fundação para a Ciência e Tecnologia (FCT) under the grants PTDC/EEI-SII/2312/2012, SFRH/BD/65248/2009 and SFRH/PROTEC/49512/2009, whose support the authors gratefully acknowledge. The authors would also like to thank the Institute for Systems and Technologies of Information, Control and Communication (INSTICC), the graphic designer André Lista, Prof. Pedro Oliveira, and the Instituto Superior de Educação e Ciências (ISEC), for their support to this work.

REFERENCES

Alves, A. P., Silva, H., Lourenço, A., and Fred, A. (2013). BITalino: A biosignal acquisition system based on arduino. In *Proceeding of the 6th Conference on Biomedical Electronics and Devices (BIODEVICES)*.

Basmajian, J. V. and De Luca, C. J. (1985). *Muscles Alive: Their Functions Revealed by Electromyography*. Williams & Wilkins, 5 sub edition.

Boucsein, W. (2011). *Electrodermal Activity*. Springer, 2nd ed. 2012 edition.

Graimann, B., Allison, B., and Pfurtscheller, G., editors (2011). *Brain-Computer Interfaces*. Springer.

Hermens, H. J., Freriks, B., Disselhorst-Klug, C., and Rau, G. (2000). Development of recommendations for sEMG sensors and sensor placement procedures. *J. of Electromyography and Kinesiology*, 10(5):361–374.

Malmivuo, J. (1995). *Bioelectromagnetism - Principles and Applications of Bioelectric and Biomagnetic Fields*. Oxford University Press, New York.

Merlo, A. and Campanini, I. (2010). Technical aspects of surface electromyography for clinicians. *The Open Rehabilitation Journal*, 3rd:98–109.

Myong-Woo Lee, Adil Mehmood Khan, T.-S. K. (2011). A single tri-axial accelerometer-based real-time personal life log system capable of human activity recognition and exercise information generation. *Springer-Verlag London Limited 2011*.

O'Sullivan, D. and Igoe, T. (2004). *Physical Computing: Sensing and Controlling the Physical World with Computers*. Thomson, 1st edition.

Webster, J. G. (2009). *Medical Instrumentation Application and Design*. Wiley, 4th edition.

Winter, D. A. (2004). *Biomechanics and Motor Control of Human Movement*. Wiley, 3rd edition.